Processing, Tensile, and Fracture Properties of Injection Molded Hdpe-Al_2O_3-HAp Hybrid Composites

Bikramjit Basu,[1] Divya Jain,[1] Nitish Kumar,[1] Pritha Choudhury,[2] Animesh Bose,[3] Shree Bose,[3] Pinaki Bose[4]

[1]*Department of Materials and Metallurgical Engineering, Laboratory for Biomaterials, Indian Institute of Technology, Kanpur*
[2]*Department of Materials Science and Metallurgical Engineering, CSJM University, Kanpur, India*
[3]*Shaping Concepts, LLC, Forth Worth, USA*
[4]*Department of Chemistry and Biochemistry, University of Texas, Arlington, Texas*

Received 7 May 2010; accepted 1 December 2010
DOI 10.1002/app.33961
Published online 21 March 2011 in Wiley Online Library (wileyonlinelibrary.com).

ABSTRACT: The aim of this study is to characterize the physical and mechanical properties of HDPE-alumina-HAp composites prepared by injection molding techniques and to demonstrate their superiority over unreinforced HDPE. Composites with up to 30 vol. % of filler, composed of equal volumes of HAp and alumina, were successfully processed by injection molding. On the basis of the analysis of processing results, i.e., melt viscosity, volume flow rate, shear rate, mixing torque, the critical ceramic loading was determined. Tensile tests done at varying crosshead speeds confirm that an increase in ceramic loading results in an increase in strength, as well as a simultaneous decrease in the total elongation at failure. A maximum strength of 20 MPa and a maximum tensile modulus of around 1 GPa was achieved with 30 vol % ceramic loading in semicrystalline HDPE matrix. SEVNB test results demonstrate an improvement in toughness at 20 vol %. The fracture properties are discussed in terms of interfacial bonding between ceramic fillers and the semicrystalline HDPE matrix. © 2011 Wiley Periodicals, Inc. J Appl Polym Sci 121: 2500–2511, 2011

Key words: injection molding; HDPE; alumina; toughness; tensile strength; modulus

INTRODUCTION

The last few decades have witnessed significant research efforts in scientific community to integrate the concepts of materials science and biological sciences to develop biomaterials for orthopedic applications[1,2] Among various biomaterials, polymer–ceramic composites are investigated to a visible extent.[3–6] The concept to produce bioactive composites for bone replacement by reinforcing a bioinert high-density polyethylene (HDPE) matrix with a bioactive HAp ceramic was first introduced in early 1980s by Bonfield,[7] and such composites are commercially known as HAPEX^{TM}. These composites have been used successfully in clinical situations as orbital implants for conditions such as postenucleation socket syndrome and orbital floor fractures.[8,9] HAp-HDPE composites have also been used successfully as middle ear implants. Dornhoffer et al.[10] designed two ossicular replacement prostheses with a HAp head and a HAp-HDPE composite shaft. The properties of these HAp-HDPE composites have also been studied extensively.[11–15] A review of available literature reveals that the HDPE-HAp composites can have a combination of properties, including E-modulus of 200–530 MPa, strength of 20–24 MPa, and strain to failure of 200–8% when fraction of HAp is varied from 10 to 50%, respectively.[16] It is recognized now that any improvement in mechanical properties of polymer–ceramic composites requires better interfacial adhesion between the reinforcement and the matrix. If load transfer is not effective across the interface, mechanical properties cannot reach expected values.

In an effort to further enhance the mechanical properties, recent research efforts are invested to develop HDPE-HAp composites with Al_2O_3 reinforcement.[4] Alumina has been chosen as the second reinforcing material because of its good biocompatibility, high wear resistance, and stability in physiological environments. Initial feasibility study was carried out using compression molding route, and the results demonstrated that improved physical properties (E-modulus, hardness), low COF, good wear resistance and, more importantly, that good cytocompatibility property (cell adhesion) can be

Correspondence to: B. Basu (bikram@iitk.ac.in).
Contract grant sponsors: Indo-US public-private joint networked center on Biomaterials for Health Care, Department of Biotechnology (DBT), Government of India.

favorably optimized by simultaneous addition of 20 vol % Al_2O_3 and 20 vol % HAp to HDPE matrix.[3–6] Therefore, it is believed that the HDPE-HAp-alumina could be a promising candidate material for orthopedic applications. Nevertheless, detailed mechanical properties in terms of tensile behavior and toughness measurements were not conducted in our earlier study and the application of such materials also demands the requirement of their processability to complex shapes using a commercially viable manufacturing route.

In this work, HDPE-HAp- Al_2O_3 composites are fabricated using injection molding, which is characterized by its ability to produce accurate complex shapes, its high production rates, and its ability to use a wide range of materials. Powder injection molding is a relatively new technology that extends the complex shaping capability of plastic injection molding into other high performance materials such as metals and ceramics.[17,18] This process has found a niche in the area of manufacturing moderately high volume of small, extremely complex shaped components from various high performance materials. The process of powder injection molding typically consist of four major steps: feedstock preparation, injection molding, debinding, and sintering. In some special cases, the actual part is the as-molded material which is made by injection molding an intimate mixture of an organic component (generally a polymer) with some inorganic powder(s). The inorganic powder can be a metal, alloy, ceramic, or a mixture of these materials. In our case, the organic component is the HDPE and the inorganic particulate material is an equal-volume mixture of alumina and HAp.

It has been now widely recognized that the injection molding is advantageous for industrial scale production of net shaped ceramic and metal products of complex shapes. The major steps involved in injection molding process are powder mixing, molding, debinding, and sintering.[19,20] Although not very popular among researchers, injection molding has been used in the past to shape biomaterials. Jaroslav and Martin[19] utilized the method for the preparation of HAp ceramics. Mondrinos et al.[21] developed a solid freeform fabrication (SFF)-based injection molding process for the fabrication of PCL and PCL-CaP scaffolds, that displayed *in vitro* cytocompatibility and suitable mechanical properties for hard tissue repair. Josepha et al.[22] addressed the effect of surface area and morphology of HAp on the rheology and processability of an injection-molding grade HAp-HDPE composite. Bakar et al.[23] reported mechanical properties of HAp-PEEK composites, produced by injection molding. Juang and Hon[20] prepared HAp ceramic bars by injection molding in an effort to study the effect of calcination temperature on the HAp powder and injection molding processability. Sahebian et al. investigated the influence of nanosized $CaCO_3$ addition on the toughness properties of HDPE nanocomposites, fabricated using injection molding.[24]

In the above perspective, the aim of this study is to show how the physical and mechanical properties of HDPE-alumina-HAp composite, prepared by injection molding route, can be better than monolithic HDPE. The composites, with varying amount of filler materials (HAp and Al_2O_3), were prepared and then tested for physical and mechanical properties, with a goal to find the optimum composition. Subsequently, SEM analysis of fractured surface was also done to study the nature of fracture, extent of debonding, distribution of phases, etc.

EXPERIMENTAL PROCEDURE

Materials preparation

In the present study, commercially available high density polyethylene (HDPE) has been used as matrix of the composite. The HDPE was from NOVA Chemicals, USA. To quantify the crystallinity of the used HDPE, Differential Scanning Calorimeter (DSC, make: Mettler) runs were carried out at 10°C/min in the temperature range of 30–180°C. Hydroxyapatite was synthesized using conventional suspension-precipitation route. The precursor materials were calcium oxide (CaO) and phosphoric acid (H_3PO_4). Initially, CaO was dispersed in distilled water with a concentration of 18.6 g/L of water. The dispersed medium was kept on a hot plate and the suspension was stirred by magnetic stirrer. Following this, an appropriate concentration (0.15*M*) of H_3PO_4 solution was added drop wise in the dispersed CaO medium. The total solution was kept stirring at 80°C for 3–4 h to allow the reaction to take place towards completion. After the completion of the reaction, the pH of the solution should be between 8 and 10. Further pH correction has been done by adding NH_4OH solution in appropriate amount. Subsequently, the solution was kept for one day to precipitate the reaction product, which was collected with the help of a filter paper. The slurry was further dried at 100°C for one day. After drying, the lump was crushed by using an agate mortar to make the material in powder form. The dried powder was calcined at 800°C for 2 h. ICP-AES (Inductive coupled plasma-atomic emission spectroscopy: spectroflame modula FTM08, Germany) analysis using complexometry technique was performed to determine the Ca/P ratio of synthesized powder. Besides HAp, commercially available alumina (α-Al_2O_3, average size: 4.8 μm, 99.4% pure, Carborumdum Universal Ltd., India) is used as another ceramic filler in the composites.

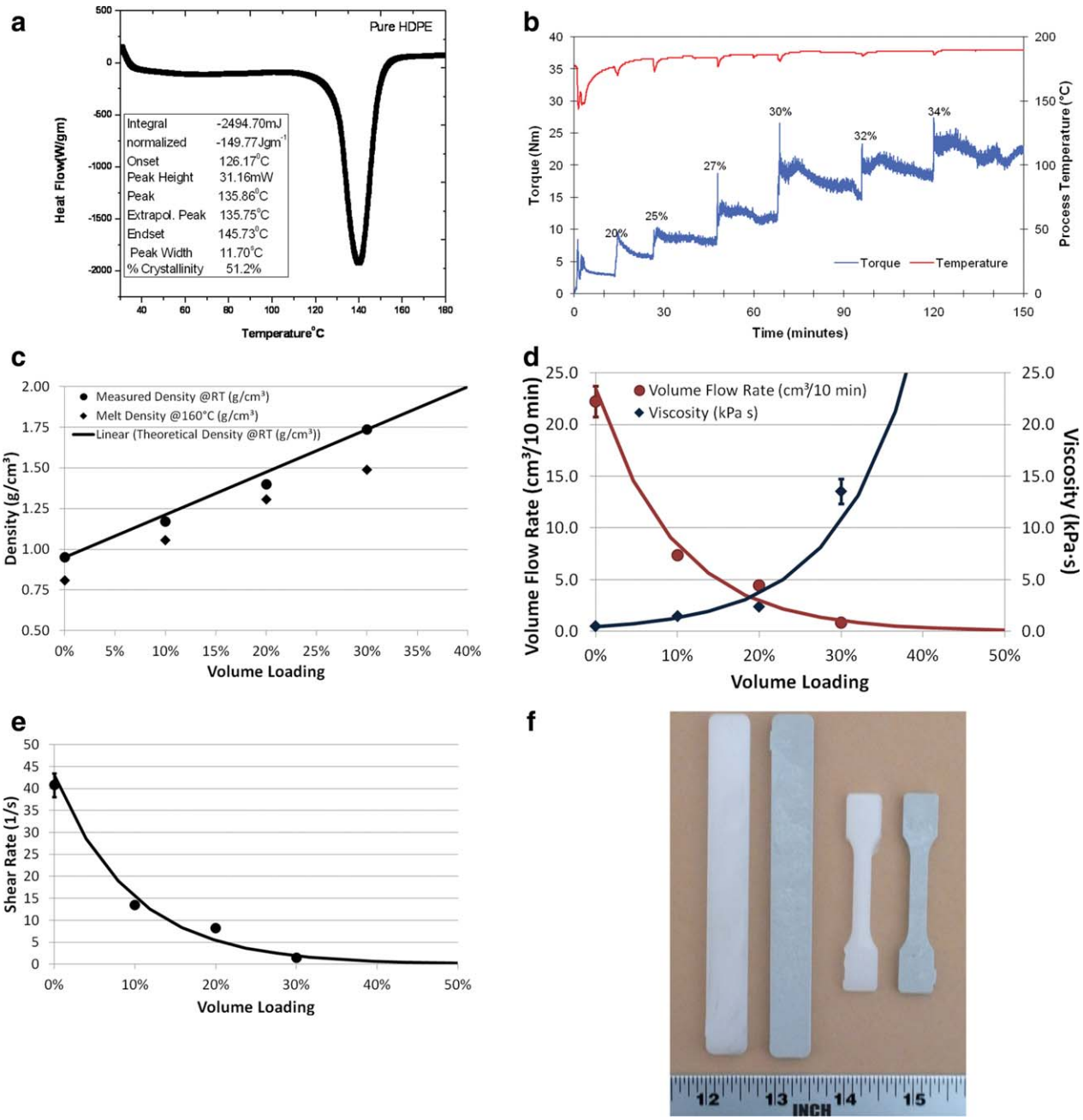

Figure 1 DSC scan of pure HDPE showing the melting endotherm (a), change in torque with solids loading (b), theoretical and experimentally measured density at RT and measured melt density at 160°C at different solids loading (c), variation of viscosity and volume flow rate with solids loading (d) and variation of shear rate with solids loading (e), bar samples of pure HDPE (far left) and HDPE + 30 vol % solid (center left) for flexural strength measurement, tensile bar of pure HDPE (center right), tensile bar of HDPE + 30 vol % solid (far right) (f). [Color figure can be viewed in the online issue, which is available at wileyonlinelibrary.com.]

As part of this study, attempts were made to maximize the ceramic filler addition to HDPE matrix using Injection molding route. A torque rheometer was used to determine the maximum solid loading that is possible using a mixture of the alumina and HAp powder (in equal volume ratio). Torque rheometry measures the change in the mixing torque with various volume loading of solid. As shown in Figure 1(b), the addition of ceramic filler is associated with a concomitant drop in the mix temperature and an increase in mixing torque. Around 34 vol % of solid addition, the mixing torque became quite erratic indicating that solid loading above this would result in an inhomogeneous mixture. It was decided that the maximum solids loading used will be 30 vol % (15 v/o alumina and 15 v/o HAp).

The mixing temperature was 170°C and the rotor speed used was 50 rpm. To systematically study the

ceramic filler addition, equal amount of HAp and alumina powders were used along with HDPE to obtain a total of 10 vol % filler, 20 vol % filler, and 30 vol % filler composites. Pure HDPE was also processed and used as a reference sample. The density of the pure HDPE, and the three other mixes with 10, 20, and 30 vol % ceramics were determined using a gas pycnometer. The volume flow rate, viscosity, and the shear rate of the four materials were determined using an Extrusion Plastometer. The extrusion plastometer investigations were carried out at 160°C using a load of 2.16 kg. Injection molding was carried out using a barrel and nozzle temperature of 160°C, a mold temperature of 40°C, pressure of 3000 psi, with a clamping force of 10 tons. During molding, the feedstock was pushed through the sprue into a runner and then into the die cavity (either a tensile bar or a flexural bar) through a gate. After injection molding, dog bone shaped tensile bars of dimension 21 mm (gauge length) × 6.35 mm (width) × 3.84 mm (thickness) as well as flexural bars of dimension 15.06 mm (width) × 5.07 mm (thickness) × 60 mm (length) were obtained. During injection molding, the melt flow characteristics, like shear rate, volume flow rate, viscosity and melt density were measured using extrusion plastometer.

Physical properties

The density values of all the samples were measured in ethanol using Archimedes's principle. For hardness measurements, a 10 g load was used to make indents on the polished surfaces; the instrument used was Vickers Hardness tester. The hardness was calculated from mean indent diagonal length by using the following standard formula, $H = 1.854\ P/d^2$ (MPa); where, P: indentation load (N), and d: arithmetic mean of the two diagonals (mm).

Mechanical properties

The tensile testing of the samples (pure HDPE and composites having 10, 20, and 30% filler) was carried out using an Instron 1195 machine at varying crosshead speeds. For all the experiments, a fixed gauge length of 21 mm was used. Three different crosshead speeds of 1 mm/min, 0.1 mm/min, and 0.05 mm/min were employed and at least three samples were used for each experiment. The data obtained were used to calculate ultimate tensile stress, elastic modulus, and total strain to failure.

Although the area under the stress–strain curves provides measures of fracture toughness, a more realistic measurement was obtained in the present study using SEVNB testing, as also followed in the work of Kim et al..[25] For this, V-notch was created on the tensile face of the 3-point bend samples by machining and a sharp crack was introduced at the notch tip using a razor blade, following ASTM standard. All the notched samples were kept in an oven at 60°C for 30 min to relieve the machining induced residual stress. The specimens were then fractured using three-point bending configuration with the span length of 50 mm and crosshead speed of 1 mm/min on Instron 1195 machine. The mode I fracture toughness, $K_{1c,}$ was determined using the following relationship.[26]

$$K_{\mathrm{Ic}} = (P_Q/BW^{1/2})\, f(x) \tag{1}$$

Where, $W = 2B$ and $x = a/W$ and $f(x) = 6 \times {}^{1/2}[1.99\text{-}\times(1\text{-}\times)(2.15\text{–}3.93\times+2.7\times^2)]/(1+2\times)(1-\times)^{3/2}$

In the above expression, a = crack length (measured using SEM on the unfractured samples), P_Q = peak load, W = width, and B = thickness. At least three samples were tested for tensile and fracture toughness property. The fractured surfaces were gold coated by a sputtering unit and observed using Scanning Electron Microscope (SEM).

RESULTS AND DISCUSSION

Processing challenges

Prior to discussing the processing results, it is important to mention the characteristics of the starting powders used in the injection molding process. X-ray diffraction (XRD) of as-synthesized HAp, calcined at 800°C reveals the characteristic X-ray peaks corresponding to pure HAp phase. A Ca/P atomic ratio of 1.66 was obtained from the HAp powder calcined at 800°C. It is important to note that, pure stoichiometric HAp possesses a Ca/P atomic ratio of 1.67. Therefore, the synthesized HAp powder is quite pure and stoichiometric. The particle size distribution was measured using laser particle size analyzer (Analysette 22; Fritsch GMBH, Germany) and the as-synthesized HAp powders have average size (d_{50}) of 1.9 μm.

A representative DSC run obtained with the used HDPE is provided in Figure 1(a). From the DSC plot, it is clear that the melting of HDPE starts at 126°C with an endotherm peak around 136°C. Total heat energy involved in the melting of HDPE is around 149.7 J/g. From the analysis of the area under the melting endotherm and knowing the total heat evolved for 100% crystalline HDPE, it was found that SCLAIR grade HDPE polymer has around 51.2% crystallinity. In Figure 1(c), both the experimental density at RT as well as melt density data at 160°C are plotted against ceramic filler addition. The experimental density is also compared

with the theoretical estimates. It is clear that the injection molding can be used to fabricate parts to near full density HDPE composites in the present case. More than 97% of theoretical density was achieved for all the samples. Also, an error in density values of 5% or less is measured. Also, an increase in the melt density with increasing ceramic filler additions is due to an increase in the amount of the powders, which have a higher density compared to the polymer (HDPE density of 0.95 g/cm^3) in the mixes. A closer look at the data in Figure 1(c) reveal that the difference in density between experimentally measured values at RT and melt density is substantial at 30 vol. % ceramic addition; whereas such difference is comparable in case of pure HDPE and 10 or 20 vol. % filler addition.

In Figure 1(d,e), the melt flow characteristics for different composite compositions are summarized. The error bars in data of Figure 1(d,e) represent the standard deviation for at least five set of experiments on each composition. It is clear from Figure 1(d,e) that both shear rate and vol. flow rate consistently decrease with increasing ceramic filler addition. As the ceramic filler content increases, the ability of the material to flow (using the same temperature and pressure) is decreased. Thus, over the same period of time, the volume flow rate of the material is decreased with increasing additions of ceramic filler. In contrast, both the viscosity and melt density systematically increase with ceramic filler addition. The viscosity of a polymeric material is generally increased with addition of particulate material, and the different feedstocks used in this study were no different. Such increase or decrease in melt flow parameter is most significant when total ceramic loading is increased from 20 to 30 vol %. For example, Figure 1(e) illustrates how the shear rate of polymeric melt decreases in a nonlinear manner with ceramic loading of up to 30 vol %. Also, the observed trend in data is also consistent with our observations that any further addition in ceramic loading beyond 30 vol % would make the melt so viscous that it would be difficult to injection mold.

Figure 1(f) shows photos of actual specimens used for flexural strength and tensile tests. Representative samples of pure HDPE and HDPE + 30 vol % solids have been shown in this figure.

The experimental measurements indicated that Vickers hardness modestly increases with an increase in filler volume fraction. This is obvious as hard ceramic particulates are distributed in a softer matrix. The hardness of the 30 vol % ceramic loaded composite was almost double (~70 MPa) than that of pure HDPE. Such hardness value is also within the range of hardness values of cortical bone (0.065–0.08 GPa).[27]

Tensile behavior

The mechanical behaviors of the polymer composites were investigated using uniaxial tensile testing of dog bone shaped samples as well as using notched samples. Figure 2 plots the tensile test results to compare the behavior at three different crosshead speeds. The elastic modulus/ultimate tensile strength (UTS)/ strain to failure data are summarized in Table I to reflect the property changes for a given material, as the crosshead speed/strain rate is changed during tensile testing. The stress-strain curve for pure HDPE, stretched in tension at 5 mm/min and 1 mm/min crosshead speeds, shows typical viscoelastic behavior of polymers [Fig. 2(a)], which is characterized by a yield point and large deformation at constant stress level at a strength value of lower than yield strength. Interestingly, a large strain to failure of around or more than 1000% was measured for pure HDPE in the present case. Such large deformation in part can be related to lower crosshead speed used in our tests as well as large crystallinity (51.2%) of the used HDPE. The tensile testing at a speed lower than 1 mm/min was not possible as the deformation exceeds the limit of the Instron machine used in the present investigation. Unlike metals, the neck does not continue shrinking until the specimen fails. Rather, the material in the neck stretches only up to a fixed drawing ratio, beyond which the material in the neck stops stretching. The neck propagates until it spans the full gauge length of the specimen and this causes high fracture strain in pure HDPE.

In contrast, the nonlinear viscoelastic deformation is highly restricted due to filler addition in HDPE and, as the amount of filler increases, the stress–strain behavior more closely resembles brittle fracture [Fig. 2(c,d)]. As discussed before, filler also influences the composite stiffness. Since the matrix is same for all the composites, the different behaviors may be attributed to the difference in filler amounts and more efficient load transfers between the filler and polymer. Typically, stiffer filler prevents the elongation of a highly ductile matrix due to efficient load transfer, ultimately decreasing the total elongation.

In view of the scale difference in terms of the total tensile deformation of the composites with respect to unreinforced HDPE, the tensile stress-strain curve of the composites at three different crosshead speeds are provided in Figure 2(b–d). Since the composite samples, particularly with higher ceramic loading, did not exhibit much nonlinear deformation at crosshead speed of 1 mm/min, all further tests were carried out at a lower speed of 0.1 mm/min and, subsequently, the lowest possible crosshead speed of 0.05 mm/min (machine limited).

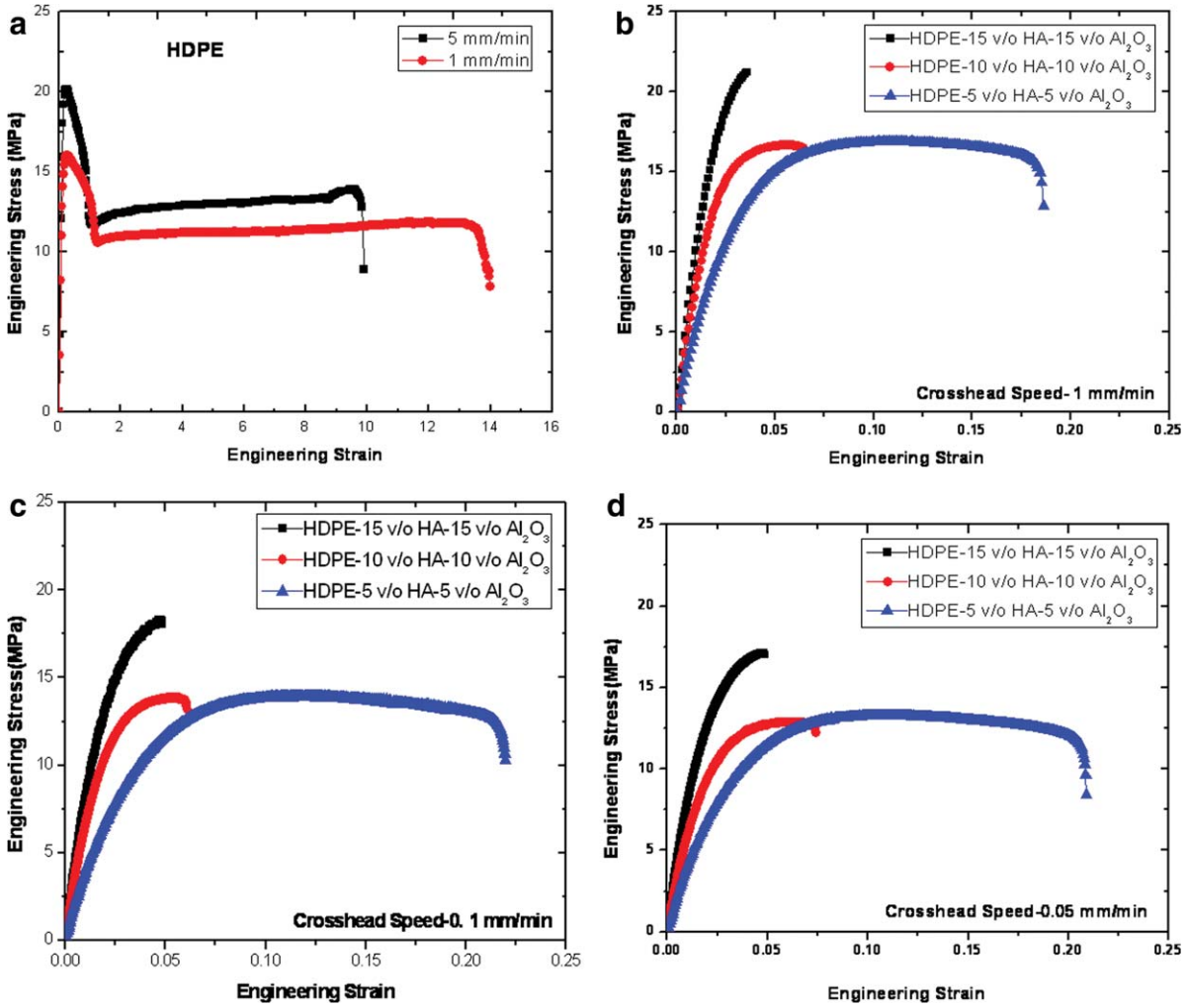

Figure 2 Engineering stress–strain plot obtained using tensile testing at varying crosshead speeds for different materials: (a) pure HDPE (b–d) HDPE-HAp-Al_2O_3 composites (composition in vol %, abbreviated as v/o). [Color figure can be viewed in the online issue, which is available at wileyonlinelibrary.com.]

TABLE I
Summary of Tensile Test Results Obtained with HDPE and its Composites, Fabricated Using Injection Molding Technique

Crosshead speed (Strain rate)	Ultimate tensile strength (MPa)	Elastic modulus (MPa)	Strain to failure (%)
Pure HDPE			
5.0 mm/min (0.004/s)	12.8	169.4	988.6
1.0 mm/min (0.0008/s)	11.3	131.3	1310.0
HDPE-5HAp-5Al_2O_3			
1.0 mm/min (0.0008/s)	16.9 ± 0.6	498.1 ± 79.9	18.6 ± 1.0
0.1 mm/min (0.00008/s)	13.9 ± 0.8	451.3 ± 15.2	22.1 ± 0.6
0.05 mm/min (0.00004/s)	13.3 ± 0.1	429.0 ± 23.8	20.1 ± 0.3
HDPE-10HAp-10Al_2O_3			
1.0 mm/min (0.0008/s)	16.7 ± 0.7	749.8 ± 202.6	6.5 ± 1.1
0.1 mm/min (0.00008/s)	13.8 ± 0.7	845.0 ± 109.7	6.1 ± 2.1
0.05 mm/min (0.00004/s)	12.9 ± 0.1	672.0 ± 3.2	7.4 ± 0.1
HDPE-15HAp-15Al_2O_3			
1.0 mm/min (0.0008/s)	21.2 ± 1.1	981.4 ± 151.4	3.5 ± .8
0.1 mm/min (0.00008/s)	18.2 ± 0.4	953.8 ± 113.3	4.8 ± 0.7
0.05 mm/min (0.00004/s)	17.1 ± 0.7	935 ± 2.1	4.8 ± 0.6

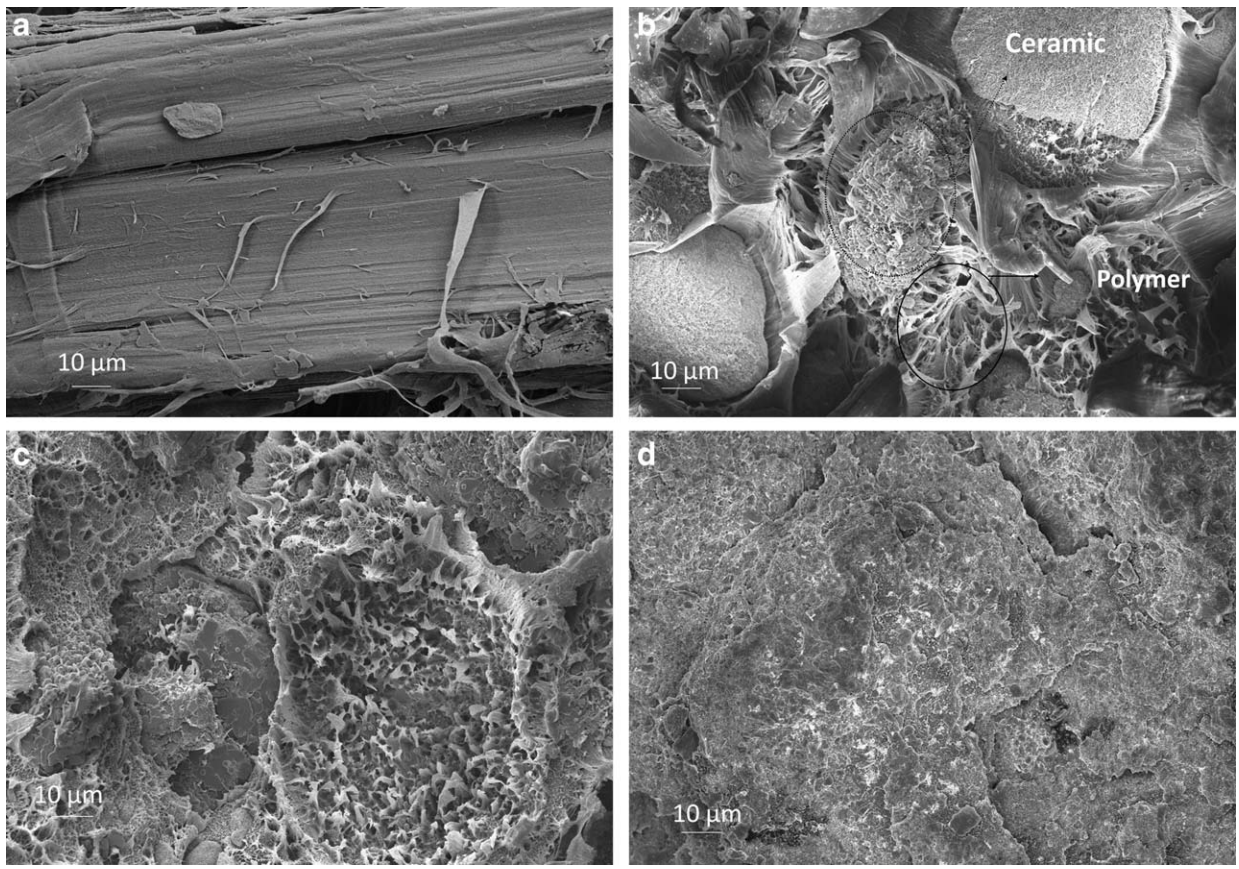

Figure 3 Representative SEM images of fracture surfaces after tensile testing at crosshead speed of 1 mm/min of (a) pure HDPE (b) HDPE with 5% alumina, 5% HAp (c) HDPE with 10% alumina, 10% HA (d) HDPE with 15% alumina, 15% HAp.

On the basis of the analysis of the tensile stress-strain curve, the elastic modulus, the ultimate tensile strength (UTS), strain to failure data are summarized in Table I. Combining Table I and Figure 2(a–d), we find that the mechanical properties are modestly dependent on strain rate of tensile testing. For example, total strain to failure for pure HDPE at crosshead speed of 1 mm/min is ~33% more than the value at 5 mm/min. Similarly, for composite samples, total strain to failure is, in general, more at crosshead speed of 0.1 mm/min than that at 1 mm/min. Overall, around two orders of magnitude lower strain to failure is recorded in the investigated composites, when compared with pure HDPE. It is clear that the strain to failure is significantly sensitive to ceramic filler addition to HDPE. For example, a sharp drop was seen even with the lowest ceramic filler addition of 10 vol % (5% of HAp and alumina, each), suggesting the significant loss of ductility. A comparison in tensile behavior at different crosshead speeds further suggests a general shift from more "ductile-like" behavior to more "brittle-like" fracture behavior, when HAp and alumina was combinedly added at 20 vol % or more. In fact, at 30 vol % ceramic loading, the tensile behavior is dominated mostly by linear elongation to fracture, a trend commonly observed with all brittle ceramics. Comparing the strain to failure values of cortical bone, that ranged from 1 to 3%,[14] our experimental results further suggest that HDPE-5 vol % HAp- 5 vol % Alumina can closely match with that of natural bone.

However, when we look at the elastic modulus values, we find that they are approximately same at three strain rates for a given composition due to overlap of the error bars. A general observation is that the ceramic filler addition of 10% can increase the E-modulus of the composite to three times compared with that of pure HDPE. The tensile modulus was seen to consistently increase with HAp and alumina content in the composite. This is expected, considering that the modulus of HAp and alumina are ~85 and ~390 GPa, respectively.[28,29] Importantly, the reinforcement effect was clearly evident even with the addition of 10 vol % of ceramic fillers. At higher filler loading of 30%, a significant increase in the modulus of about sixfold was observed as compared to pure HDPE. It may be noted that a maximum elastic modulus of close to 1 GPa has been

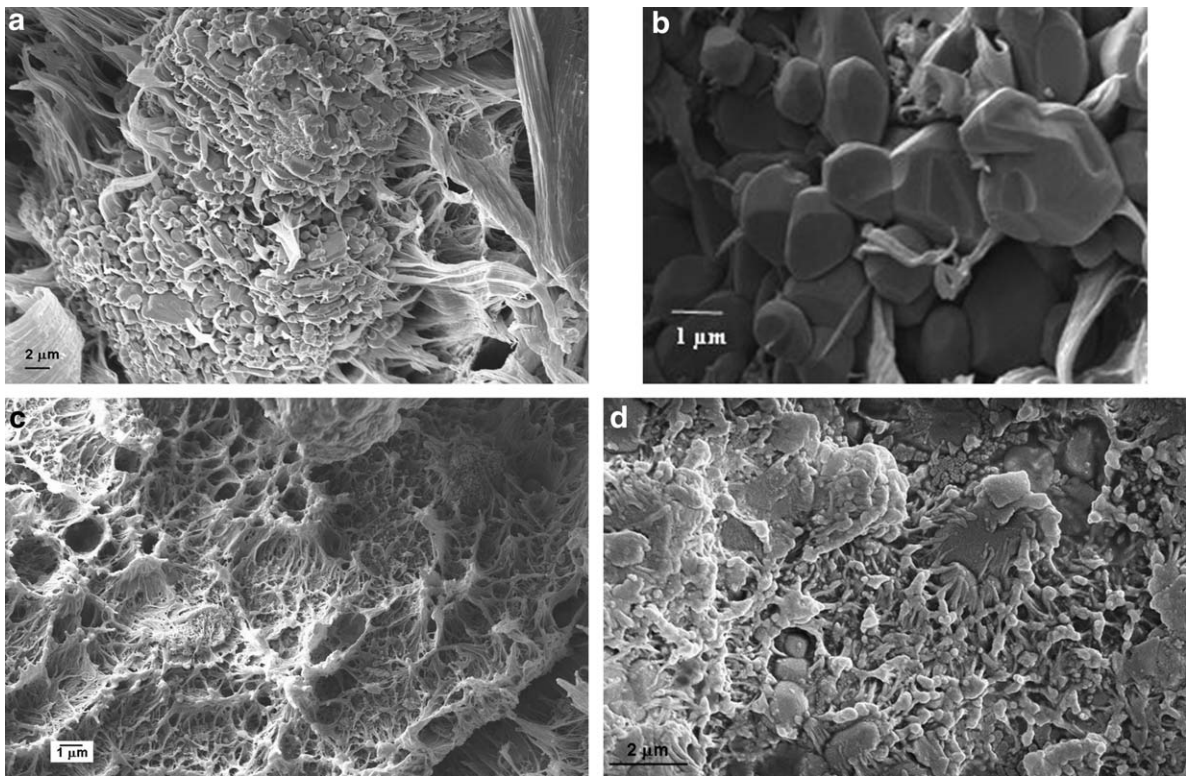

Figure 4 SEM images of fracture surfaces obtained after tensile testing at crosshead speed of 1 mm/min showing (a) alignment of fracture surface along tensile axis (10% filler) (b) particle–particle bonding in 20% filler composite (c) wave kind of pattern on fracture surface (20% filler) and (d) 30% filler composite showing brittle kind of fracture.

measured with 30% ceramic loaded HDPE composite, which is still lower than the lower bound elastic modulus of natural cortical bone (2–3 GPa).[16]

As far as the ultimate tensile strength property is concerned, we do notice a clear decrease in UTS with strain rate for a given investigated material. Also, such a decrease in UTS with a corresponding decrease in crosshead speed is comparable for three composite compositions. For example, the composites with 10, 20, and 30% ceramic loading exhibit ~18, 17, and 14% decrease in UTS, respectively, as strain rate is decreased from 1 mm/min to 0.1 mm/min. While the UTS of 10 and 20% ceramic loaded HDPE composites at various strain rate are comparable to each other, UTS of 30% loaded samples are significantly higher (two times) than pure HDPE. A strength value of more than 20 MPa is achievable in HDPE-15 HAp-15 alumina composites.

Fracture mechanisms

Figure 3(a) shows a typical fracture surface of pure HDPE polymer, revealing the parallel orientation of bundles of HDPE fibers along the tensile stress axis. Figure 3(b) shows the fracture surface of composite having 10% filler (5% HAp and 5% alumina) volume. It shows debonding at ceramic-polymer interface, which is one of the important mechanisms for energy dissipation during fracture. As amount of filler volume increases, the interface area also increases. As a result, the chance of debonding during fracture also increases which is the reason for increasing fracture toughness with filler volume. Figure 3(c) shows the fracture surface of 20% filler (10% HAp and 10% alumina) composite. The interfacial debonding, fiber pull out (ceramic particles) and fibrous nature of polymers can be observed on Figure 3(c). In contrast, brittle like fracture behavior of 30% ceramic (15% HAp and 15% alumina) loaded composite can be seen in Figure 3(d).

More information on the fracture characteristics was obtained from higher magnification SEM images, as shown in Figures 4–6. Figure 4 shows representative SEM images obtained after tensile testing at 1 mm/min crosshead speed. Interestingly, the agglomeration of both the ceramic fillers could be observed on fracture surfaces, as seen on Figure 4(a). Such observations indicate that the fracture plane mostly contains such agglomerates of ceramic fillers and we believe that ceramic fillers, being brittle, can not take increased load in tension, leading to brittle-like behavior. In Figure 4(b), the uniform dispersion of ceramic fillers is observed and such distribution restricts the nonlinear deformation of

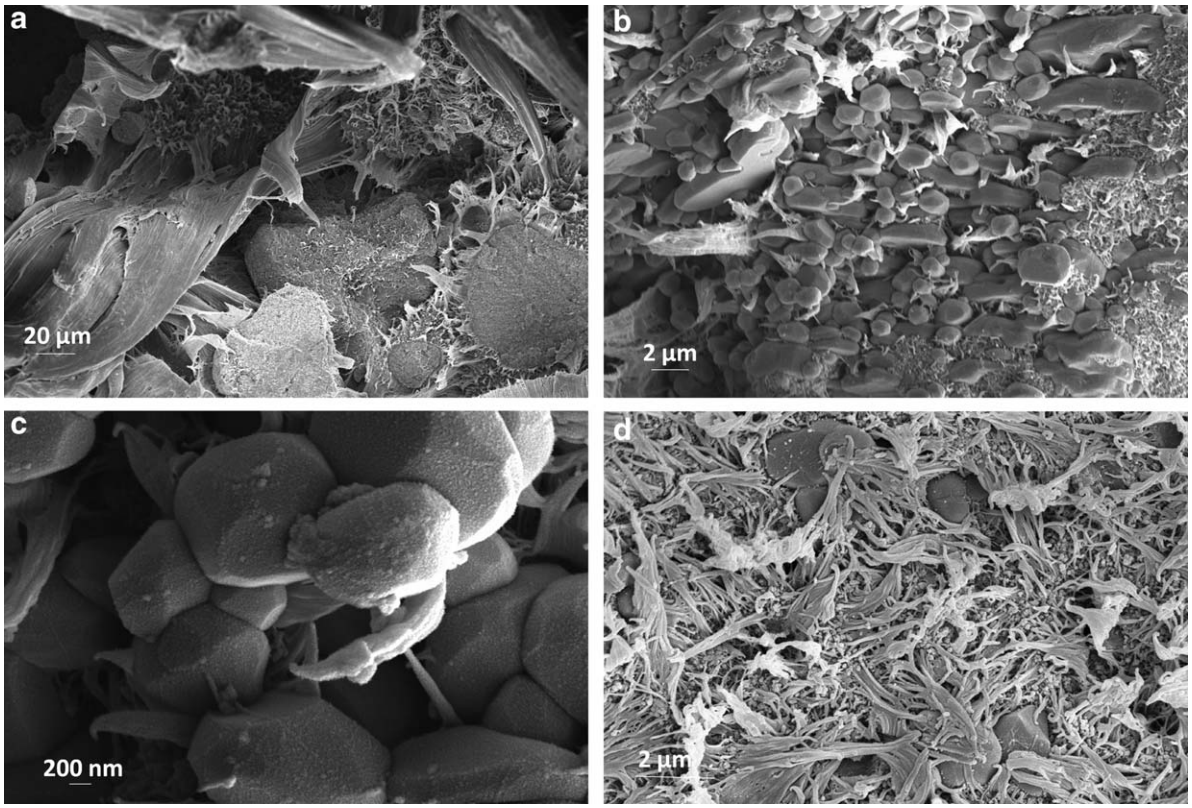

Figure 5 SEM images of fracture surfaces obtained after tensile testing at crosshead speed of 0.1 mm/min, showing (a) long deformation characteristic of polymers (10% filler) (b) alignment of fracture surface along tensile axis (20% filler) (c) particle-particle bonding (20% filler) (d) brittle kind of fracture with very less deformation (30% filler)

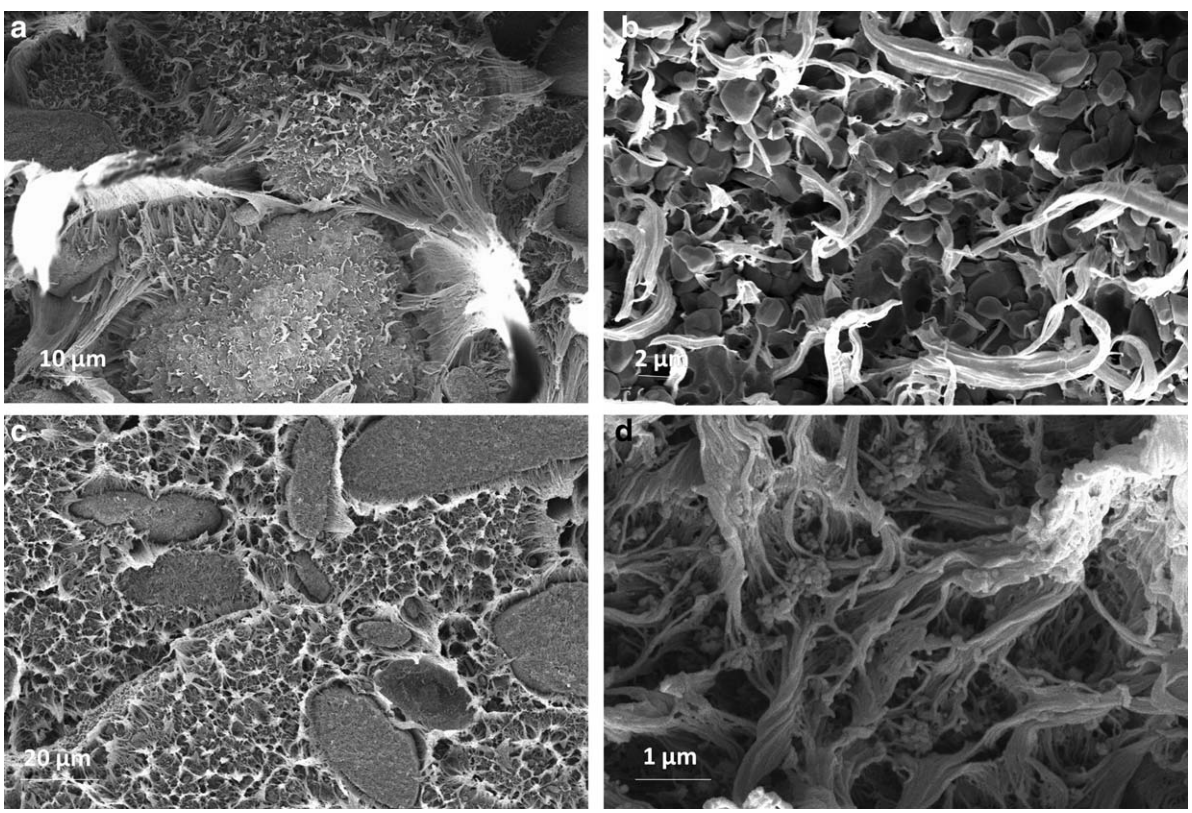

Figure 6 SEM images of fracture surfaces obtained after tensile testing at crosshead speed of 0.05 mm/min showing (a) long deformation characteristic of polymers (10% filler) (b) uniform distribution of ceramic phase in polymer matrix (10% filler) (c) ceramic particles embedded in polymer matrix and fiber pullout (20% filler) (d) clusters of ceramic particles which impede polymer elongation (20% filler).

polymeric fibers. A completely random arrangement of polymer fibers is clearly visible in Figure 4(b). Interestingly, Figure 4(c) indicates good particle-to-particle bonding in microstructural regions loaded with ceramic fillers. Although the temperature of the ceramic loaded polymer melt during injection molding did not reach more than 300°C, the neck formation and good bonding reveals advantageous properties of injection molding process. In fact, such particle arrangement is commonly observed in fully dense ceramics. In Figure 4(c), the wavy pattern of fracture surface of 20% ceramic loaded HDPE composite could be observed. Such pattern essentially reflects plastic deformation prior to fracture. In 30% ceramic loaded composite, the ceramic fillers are mostly observed to be attached to short polymeric chains.

At a smaller crosshead speed of 0.1 mm/min, some new features to the deformation behavior could be noticed. While the HDPE fiber pull out and pockets of ceramic fillers could be noticed on 10% filler composite fracture surface [Fig. 5(a)], the alignment of ceramic fillers along tensile axis could be critically noted in case of 20% ceramic filler loaded composites [Fig. 5(b)]. It is possible that the presence of viscoelastic polymer matrix allows the ceramic particle to rotate and accommodate themselves along tensile axis. Like in Figure 3(c), the dense arrangement of ceramic fillers could be noticed on the fracture surface in Figure 4(c). At higher ceramic loading of 30 vol %, random arrangement of polymeric fibers without any marked deformation features could be noticed in Figure 4(d).

Figure 5(a) shows a region of fracture surface of 20% filler composite. Here we can observe ceramic particles coalescing into each other and forming a neck-like feature which is characteristic of the sintering process. Such features were not observed in 10% filler composite, which tells that these form only at higher volume fraction of ceramics in the polymer phase. Figure 5(b) shows a wave kind of pattern on the fracture surface, which is a characteristic of such composites only. Figure 5(d) shows the fracture surface for 30% filler composite. It also confirms homogeneity of phase distribution by injection molding route. However, there is no wavy nature of fracture surface and also the fibrous nature of polymer matrix is not prominent, which confirm its brittle nature of failure. While similar fracture morphologies were also observed at lowest crosshead speed of 0.05 mm/min, a clear observation of the presence of the ceramic fillers in between the polymeric fibers could be noticed in 30% ceramic loaded HDPE composite [Fig. 6(d)].

In this work, the matrix of the composite is semicrystalline HDPE. Fundamentally, the tensile deformation behavior of such polymers involves the stretching, or the elongation, of the polymeric fibers in the amorphous region towards and along the loading direction. From the observations of Figures 3–6, it is expected that ceramic fillers are favorably placed in between entangled chains in the polymer matrix. Such arrangement presumably prevents the sliding of long polymeric chains during tensile deformation. Mechanistically, such phenomenon helps in establishing "physical crosslinking" of polymer chains, which would substantially reduce the chain mobility and encourage entanglement. Moreover, the presence of alumina in the polymeric matrix restricts the permanent deformation, which results in considerable increase in hardness/strength values than that of pure HDPE. Additionally, the mechanical interlocking is expected by the shrinkage of the polymer matrix onto the filler particles during cooling of the composites after injection molding.

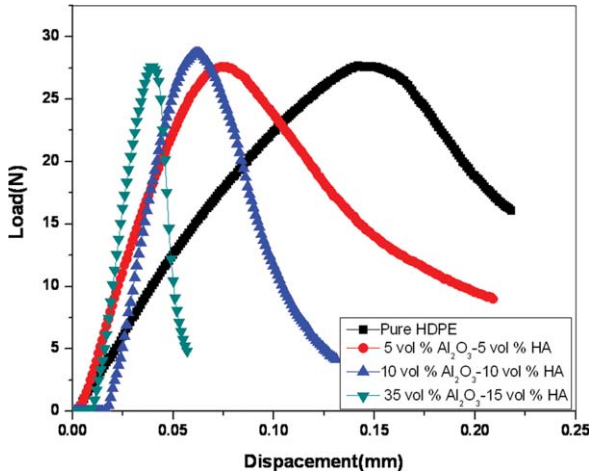

Figure 7 Load-Displacement plot obtained for 3-point bend test for fracture toughness measurement at crosshead speed of 1 mm/min for different materials: pure HDPE, HDPE-HAp-Al_2O_3 composites (10, 20, and 30 vol %). [Color figure can be viewed in the online issue, which is available at wileyonlinelibrary.com.]

Notched behavior in flexure

A number of experimental methods are available for the measurement of fracture toughness.[30] In the present case, long crack toughness method, i.e., SEVNB testing is adopted and the notched samples with a sharp precrack are fractured in 3-point flexure mode. The recorded load-displacement data are plotted in Figure 7. Qualitatively, a general observation is that the initial linear mechanical response in flexure goes through a nonlinear response prior to attaining the peak value, beyond which the notched samples can not sustain any increased load. Although the load drops in a nonlinear manner, the entire flexure sample was not broken in case of pure HDPE and 10 or 20 vol % filler

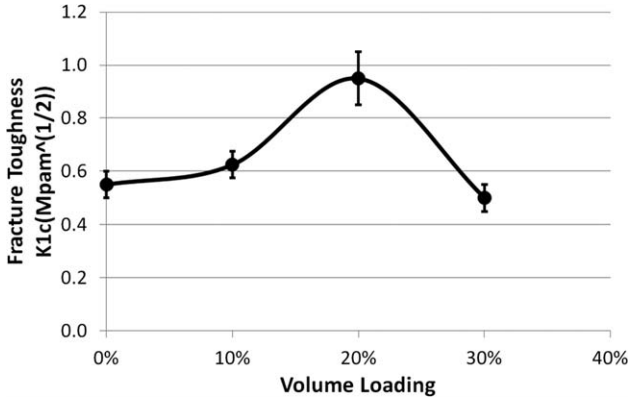

Figure 8 Plot of fracture toughness, as measured using SEVNB testing, with vol % ceramic loading to HDPE.

addition. An important observation is that the peak load is attained at lower displacements, as the filler addition is increased and therefore, the load-displacement curve is shifted more towards left. Similar observations have been made in case of HDPE-$CaCO_3$ nanocomposites with the exception that the peak load is decreased with the second phase addition.[24]

On the basis of eq. (1), the mode I fracture toughness was determined and plotted in Figure 8. The obtained fracture toughness was in the range 0.55–1.0 MPa.$m^{1/2}$, which is close to the lower bound of natural cortical bone fracture toughness (2–6 MPa $m^{1/2}$).[31] It is clear from Figure 8 that an enhancement in fracture toughness is only realized at the ceramic loading of 20 vol %. An increase in the fracture toughness essentially indicates better energy dissipation at 20 vol % solid loading. In general, a number of mechanisms contribute to the fracture toughness and it is often very difficult to determine the dominant mechanism.[32] In case of HDPE-based composites, the major energy absorption mechanisms include crack deflection, debonding between fiber and matrix, pull-out (extraction of fibers from the matrix), and fiber-bridging mechanism.[33] Some selected SEM images of the fracture surfaces after SEVNB testing are provided in Figure 9. In Figure 9(a), the alignment of HDPE fibers in the crack tip process zone is clearly observed. Also, the debonding at alumina particle/polymer interface can be clearly observed in Figure 9(b). Similar, polymer-filler particle interfacial debonding is also noticed in other composite compositions.

At closure, one important point to note here is that we have successfully injection molded HDPE composites with 30% ceramic loading. This is in contrast with earlier attempts to make HAp composites using injection molding, where it was reported that without the use of additives, good mixing beyond 20% HAp loading was difficult[34]. Another point that needs to be mentioned is that we have measured much lower elastic modulus in injection molded HDPE composites as compared with compression molded composites, reported in our earlier work.[4] Such a difference can be attributed to the difference in the measurement technique. The compression molded samples were tested using the instrumented hardness tester at low load of less than 1*N* and consequently, microscopically smaller volumes were tested at indented regions. From the unloading response at such a small microstructural volume, the elastic modulus was calculated. In this case, the bulk elastic modulus was calculated from the slope of the linear part of the stress–strain curve and therefore, these values are more realistic.

As a concluding note, it can be stated that an amount of ceramic fillers in the range of 10–20 vol % appears to be optimal in terms of strength and toughness. From the processing aspect, HDPE with 10–20 vol % fillers can be injection molded into complex shapes without any major problems. From the present investigation, it appears that, due to the size and shape of the given particles, injection molding

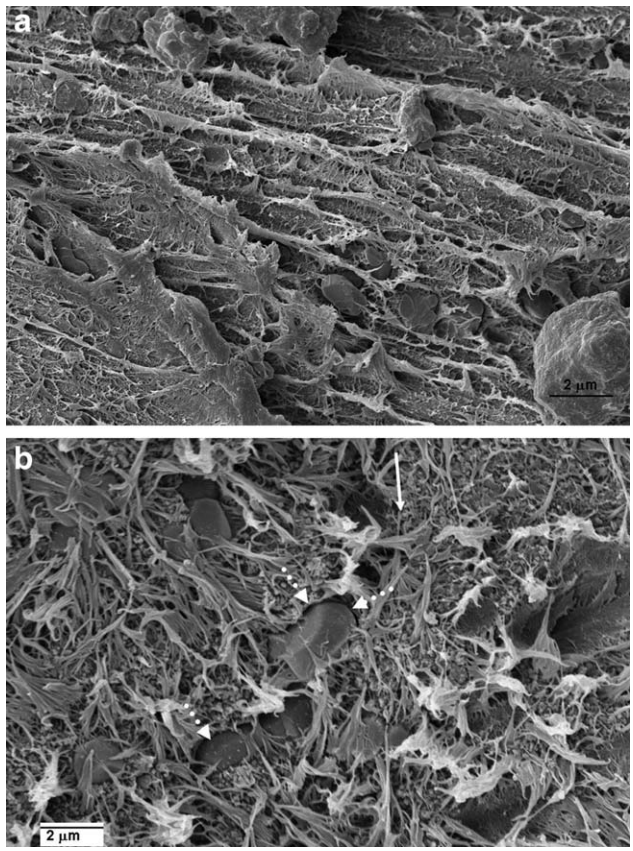

Figure 9 Representative SEM images illustrating the observation of alignment of polymeric chains around the crack tip stress field adjacent to the V notch after SEVNB testing (a) and debonding of alumina platelets, indicated by dotted arrow during the propagation of the primary crack (bold crack). Both the images are obtained in case of 10 vol % ceramic loaded composite.

cannot be used as a fabrication process for ceramic loading of more than 30 vol %. However, with different particulate morphology (spherical), size and size distribution, it is possible to achieve greater loadings than 30 vol %.

Since various biomedical applications require the availability of biocompatible materials in different shapes, the ability to produce injection molded components will open us new opportunities with the HDPE-alumina-HAp system. Currently, the materials are being tested for their biological response.

CONCLUSIONS

Based on the experimental results, the following major conclusions can be drawn:

a. On the basis of the torque rheometry study, HDPE composites with a maximum solid loading of up to 30 vol. % (equal volume fraction of HAp and alumina) can be processed to theoretical density using the injection molding route.
b. The extrusion plastometer measurements indicate that with increase in volume fraction of solids loading, the shear rate and volume flow rate both decreases, while the viscosity increases.
c. The tensile test results reveal that a maximum tensile strength of more than 20 MPa and tensile modulus of close to 1 GPa is achievable with 30% ceramic loaded HDPE composite. However, such property enhancement is accompanied by significant reduction in total strain to failure, as compared to unreinforced HDPE. This has been explained in terms of more difficulty in chain mobility of semicrystalline HDPE matrix in the presence of ceramic fillers. Also, an increase in ceramic loading from 10 to 20 vol. % does not increase the tensile strength. Another observation is that the tensile strength increases with increase in strain rate, independent of the composite composition.
d. SEVNB fracture toughness data reveal a maximum toughness of close to 1 $MPa{\cdot}m^{1/2}$ in 20% ceramic filler loaded HDPE. However, a lower toughness is measured at 30 vol % ceramic loaded HDPE.
e. The microstructural characterization of the fracture surface topography indicated considerable plastic deformation of HDPE matrix and debonding along polymer/alumina platelet interface. The uniform distribution of submicron HAp particles in between polymeric chains is commonly noticed.

References

1. Basu, B.; Katti, D.; Kumar, A. Advanced Biomaterials: Fundamentals, Processing and Applications; Wiley: USA, 2009.
2. Ratner, B. D.; Hoffman, A. S.; Schoen, F. J.; Lemons, J. E. Biomaterials Science: An Introduction to Materials in Medicine; Elsevier Academic Press: London, 2004.
3. Bodhak, S.; Nath, S.; Basu, B. J Biomater Appl 2009, 23, 407.
4. Nath, S.; Bodhak, S.; Basu, B. J Biomed Mater Res: Part B Appl Biomater 2009, 88, 1.
5. Bodhak, S.; Nath, S.; Basu, B. J Biomed Mater Res A 2008, 85, 83.
6. Nath, S.; Bodhak, S.; Basu, B. J Biomed Mater Res A 2007, 83, 191.
7. Bonfield, W.; Grynpas, M. D.; Tully, A. E.; Bowman, J.; Abram, J. Biomaterials 1981, 2, 185.
8. Downs, R. N.; Vardy, S.; Tanner, K. E.; Bonfield, W. Bioceramics 1991, 4, 239.
9. Bonfield, W. Bioceramics 1998, 11, 37.
10. Dornhoffer, J. L. Laryngoscope 1998, 108, 531.
11. Huang, J.; Di Silvio, L.; Wang, M.; Tanner, K. E.; Bonfield, W. J Mater Sci 1997, 8, 775.
12. Suwanprateeb, J.; Tanner, K. E.; Turner, S.; Bonfield, W. J Mater Sci 1997, 8, 469.
13. Suwanprateeb, J.; Tanner, K. E.; Turner, S.; Bonfield, W. J Biomed Mater Res 1998, 39, 16.
14. Wang, M.; Joseph, W. B. Biomaterials 1998, 19, 2357.
15. That, T.; Tanner, K. E.; Bonfield, W. J Biomed Mater Res 2000, 51, 453.
16. Pandey, A.; Jan, E.; Aawath, P. B. J Mater Sci 2006, 41, 3369.
17. German, R. M.; Bose, A. Injection Molding of Metals and Ceramics; Metal Powder Industries Federation: Princeton, NJ, 1997.
18. Mutsuddy, B. C.; Ford, R. G. Ceramic Injection Molding; Chapman and Hall Inc.: New York, NY, 1995.
19. Cihlar, J.; Trunec, M. Biomaterials 1996, 17, 1905.
20. Juang, H.; Hon, M. Ceram Int 1997, 23, 383.
21. Mondrinosa, M. J.; Dembzynskib, R.; Lub, L.; Byrapogub, V. K. C.; Woottonb, D. M.; Lelkesa, P. I.; Zhoub, J. Biomaterials 2006, 27, 4399.
22. Josepha, R.; McGregora, W. J.; Martynb, M. T.; Tannera, K. E.; Coatesb, P. D. Biomaterials 2002, 23, 4295.
23. Abu Bakar, M. S.; Cheang, P.; Khor, K. A. Compos Sci Technol 2003, 63, 421.
24. Sahebian, M.; Gebarjad, S. M.; Sajjadi, S. A.; Sherafat, Z.; Lazzeri, A. J Appl Polym Sci 2007, 104, 3688.
25. Kim, B.; Park Lee, S. W. Compos Struct 2008, 86, 69.
26. ASTM D5045-99. Standard test methods for plane-strain fracture toughness and strain energy release rate of plastic, American Society for Testing and Materials (ASTM); 2007.
27. Wang, X. J.; Chen, X. B.; Hodgson, P. D.; Wen, C. E. Trans Nonferrous Met Soc China 2006, 16, 744.
28. Wang, M.; Porter, D.; Bonfield, W. Br Ceram Trans 1994, 93, 91.
29. Li1, G. H.; Hu, Z. X.; Zhang, L. D.; Zhang, Z. R. J Mater Sci Lett 1998, 17, 1185.
30. Kovarik, R. E.; Fairhurst, C. W. Dent Mater 1993, 9, 222.
31. Yan, J.; Clifton, K. B.; Mecholsky, J.; John, J.; Reep, R. L. J Biomech 2006, 39, 1066.
32. Matthews, F. L.; Rawlings, R. D. Composite Materials: Engineering and Science; Chapman and Hall: London, 1994.
33. Silva, R. V.; Spinelli, D.; Bose Filho, W.W.; Claro Neto, S.; Chierice, G. O.; Tarpani, J. R. Compos Sci Technol 2006, 66, 1328.
34. Sim, C. P.; Cheang, P.; Liang, M. H.; Khor, K. A. J Mater Proc Technol 1977, 69, 75.